Electronic Supporting Information for:

Enhancement of Magnetic Anisotropy in a Mn-Bi Heterobimetallic Complex

Tyler J. Pearson[†], Majed S. Fataftah[†], and Danna E. Freedman*[†]

[†]*Department of Chemistry, Northwestern University, Evanston, Illinois 60208-3113*

Table of Contents

General Considerations. Manipulations of all compounds were performed under a dinitrogen atmosphere in a Vacuum Atmospheres Nexus II glovebox unless otherwise specified. Glassware was either oven-dried at 150 ^{o}C for at least 4 hours or flame-dried prior to use. Acetonitrile (MeCN), diethyl ether (Et_2O), tetrahydrofuran (THF), and dichloromethane (DCM) were dried using a commercial solvent purification system from Pure Process Technology and stored over 3 or 4 Å molecular sieves prior to use. Methanol (MeOH) was also dried and degassed on the solvent system, but was distilled prior to use to remove residual sieve dust. Butyronitrile was distilled from CaH_2, degassed via three consecutive freeze-pump-thaw cycles, and stored over 4 Å molecular sieves prior to use. 1,1,1-tris(aminomethyl)ethane hydrochloride (TAME*3HCl) was prepared by the method described by Ralph et. al.[1] All other reagents were used as received.

[1,1,1-tris[(3-methoxysalicylideneamino)methyl]ethane] (H_3L). An adaptation of a literature procedure was used to isolate **H_3L**.[2] In air, TAME*3HCl (1.28 g, 5.6 mmol) was stirred into a slurry in 100 mL MeOH in a 500 mL round bottom flask. To this slurry 100 mL of a MeOH solution of NaOH (0.72 g, 18.1 mmol) was added. This solution was allowed to stir for approximately 10 minutes until the solution turned clear and colorless. A 70 mL MeOH solution of *ortho*-vanillin was then added (2.57 g, 16.9 mmol). After being allowed to stir for 2 hours, the solvent was removed *in vacuo* and the residue was extracted with 50 mL DCM. This extract was vacuum filtered to remove precipitate. The solution was subsequently filtered again through a pad of celite. The DCM was then removed *in vacuo* to yield a yellow powder. 1.88 g (3.6 mmol, 64% yield). ^{1}H NMR (500 MHz, dimethyl sulfoxide-d_6) – δ 1.06 (s, 3H, CH_3), 3.62 (s, 6H, CH_2), 3.29 (s, 9H, CH_3), 6.83 (t, J = 8 Hz, 3H, Ar-CH), 7.03 (d, J = 8 Hz, 3H, Ar-CH), 7.06 (d, J = 8 Hz, Ar-CH), 8.58 (s, 3H, CH), 13.65 (br s, 2H, Ar-OH)

$[Mn^{II}(L)Bi^{III}](OTf)_2$. In a 20 mL vial in an N_2 glovebox 144.3 mg (0.28 mmol) of **H_3L** was dissolved in 6 mL THF and stirred. To this mixture was added a solution of 46.4 mg (0.86 mmol) NaOMe in 3mL MeOH. This was allowed to stir for 30 minutes. After 30 minutes, a solution of 99.1 mg (0.28 mmol) $Mn(OTf)_2$ in 3mL MeOH was added. The yellow solution gradually turned orange, and was permitted to

stir overnight. The next day, the solvent was removed in vacuo to yield an orange powder. This powder was taken up in 5 mL DCM, filtered through a plug of celite, and then the DCM was removed *in vacuo*. This residue was then dissolved in 5 mL THF and, while stirring, a solution of 182.8 mg (0.28 mmol) $Bi(OTf)_3$ in 3mL THF was added dropwise. This reaction was allowed to proceed overnight. The next day, the reaction was filtered through a Buchner funnel and the yellow precipitate was collected. This was purified *via* recrystallization through vapor diffusion of Et_2O into a MeCN solution to yield 105.5 mg (33 %) of crystalline product. IR: 2951(w), 2898(w), 2851(w), 1620(s), 1606(s), 1566(s), 1469(s), 1455(s), 1441(vs), 1402(s), 1388(s), 1367(m), 1316(s), 1281(s), 1265(s), 1239(w), 1225(w), 1190(s), 1167(w), 1075(s), 1030(vs), 1003(s), 965(s), 947(s), 907(m), 845(s), 785(m), 734(s), 629(s), 604(m), 571(m), 513(s), 474(s), 423(m), 411(m) ESI-MS: $[C_{29}H_{30}N_3O_6MnBi(OCH_3)]^+$ m/z = 811.12; Elemental Analysis: Calculated % (Found %), C: 34.52 (34.52), H: 2.80 (2.78), N: 3.90 (3.76)

Magnetic Measurements: All samples were prepared under inert atmosphere and were measured in flame-sealed quartz tubes. Samples were prepared from ground microcrystalline material which was restrained in molten eicosane to prevent torqueing of crystallites. All measurements were conducted on a Quantum Design MPMS-XL SQUID magnetometer from 1.8 to 300 K and applied dc fields of 0-7 T. Diamagnetic corrections for the sample holder and diamagnetism intrinsic to the sample were calculated from Pascal's constants. Prior to full characterization, magnetisation from 0-4 T at 100 K was measured. Linear behavior in this curve indicated no ferromagnetic impurities. Data agreement was checked between multiple measurements. Fits and simulations were performed with the MagProp package within DAVE 2.0.[3]

EPR Measurements: All samples were prepared under inert atmosphere and were measured in flame-sealed quartz tubes. Samples were prepared from ground microcrystalline material which was prepared as a 0.1 mM solution in butyronitrile. Simulations to experimental data were performed using EasySpin.[4]

X-ray Diffraction Studies: Single crystals suitable for X-ray analysis were coated with Paratone N oil and mounted on a MiTeGen MicroLoop™ for analysis. Data were collected at 100 K on a Bruker

KAPPA APEX diffractometer equipped with a MoKα microsource, a Quazar™ Optics monochromator, and a Bruker APEX II CCD area detector. Raw data were integrated and corrected for Lorentz and polarization effects using Bruker Apex2 v. 2014. 11.[5] Absorption corrections were applied using SADABS.[6] Space group assignments were determined through examination of systematic absences, E-statistics, and successive refinement of the structures. Structures were solved using direct methods in SHELXT and further refined with SHELXL-2013[7] operated with the OLEX2[8] interface.

Other Physical Measurements: Elemental analysis was performed by Midwest Microlab (Indianapolis, IN). Infrared spectroscopy was performed on a Bruker Alpha FTIR spectrometer equipped with an attenuated total reflectance accessory. Solution-phase NMR spectroscopy was performed using a Varian Inova 500 MHz spectrometer. ^{1}H NMR spectra were referenced to the DMSO residual peak at 2.50 ppm. Electrospray mass spectra were collected in both positive and negative ionization mode on a Bruker AmaZon SL spectrometer equipped with a quadrupole ion trap using MeCN as the carrier solvent.

Discrepancy in *g*-values between magnetometry and EPR: The differences in the simulated *g*-values between the magnetometry measurements and the EPR measurements arise from two sources. Primarily, it is difficult to account for *g*-anisotropy in magnetometry of powdered samples without overparameterizing the model, which is why simulation of magnetometry data proceeded with an isotropic *g*-value. Second, where simulation of EPR spectra does not depend upon sample quantity or absolute intensity, magnetometry is extremely quantity-dependent, creates different sources of error for the separate measurements.

Table S1. Crystallographic information for the structural refinement of **2**.

Empirical Formula	$C_{31}H_{30}BiF_6MnN_3O_{12}S_2$
Formula weight	1078.62 g/mol
Temperature	100 K
Wavelength	0.71073 Å
Crystal System	Triclinic
Space Group	*P*–1
Unit Cell Dimensions	a = 9.6023(5) Å, α = 96.095(3)˚
	b = 12.8674(7) Å, β = 105.256(3)˚
	c = 16.9332(9) Å, γ = 104.605(3)˚
Volume	1806.25(17) Å^3
Z	2
Density (calculated)	1.983 Mg/m^3
Absorption coefficient	5.43 mm^{-1}
F_{000}	1054
Crystal color	Yellow
Crystal size	0.087 × 0.070 × 0.034 mm^3
θ range	1.358 – 30.233˚
Index ranges	$-13 \le h \le 13$
	$-18 \le k \le 18$
	$-22 \le l \le 22$
Reflections collected	73675
Independent reflections	10716 [R_{int} = 3.14]
Completeness to θ = 30.233˚	99.5%
Absorption correction	Multi-scan
Maximum and minimum transmission	0.680, 0.746
Refinement method	Full-matrix least-squares on F^2
Data / restraints / parameters	10716 / 64 / 552
Goodness-of-fit on F^2[a]	1.034
Final R indices [I > 2σ(I) = 10626 data][b]	R_1 = 3.35 %, wR_2 = 7.33 %
R indices (all data, 0.80 Å)	R_1 = 4.33 %, wR_2 = 7.59 %
Largest diff. peak and hole	3.84 and –1.31 e.Å^{-3}

[a] GooF = $[\Sigma[w(F_o^2-F_c^2)^2] / (n-p)]^{1/2}$ where n is the number of reflections and p is the total number of parameters refined. [b] $R_1 = \Sigma||F_o|-|F_c|| / \Sigma|F_o|$; $wR_2 = [\Sigma[w(F_o^2-F_c^2)^2] / \Sigma[w(F_o^2)^2]\ ]^{1/2}$

Monometallic complex[2]		Complex 2 (this work)		N6 Claterochelate[9]	
Bond Lengths					
N1-Mn	2.259(2)	N1-Mn	2.145(3)	N1-Mn	2.2721(38)
N2-Mn	2.243(2)	N2-Mn	2.175(3)	N2-Mn	2.2207(40)
N3-Mn	2.264(2)	N3-Mn	2.148(3)	N4-Mn	2.2371(37)
O1-Mn	2.1490(18)	O1-Mn	2.199(2)	N5-Mn	2.2286(42)
O2-Mn	2.117(2)	O2-Mn	2.132(2)	N7-Mn	2.2799(35)
O3-Mn	2.111(2)	O3-Mn	2.201(2)	N8-Mn	2.2112(38)
Bond Angles					
N1-Mn-N2	85.12(8)	N1-Mn-N2	84.99(12)	N1-Mn-N2	71.635(136)
N1-Mn-N3	78.94(8)	N1-Mn-N3	87.74(11)	N4-Mn-N5	71.744(143)
N2-Mn-N3	83.06(8)	N2-Mn-N3	91.24(11)	N7-Mn-N8	71.262(138)
O1-Mn-O2	89.55(7)	O1-Mn-O2	75.37(9)	N1-Mn-N7	76.124(133)
O1-Mn-O3	89.13(7)	O1-Mn-O3	75.58(9)	N1-Mn-N4	77.947(136)
O2-Mn-O3	89.35(8)	O2-Mn-O3	74.02(9)	N4-Mn-N7	78.782(141)
N1-Mn-O1	80.39(7)	N1-Mn-O1	82.90(10)	N2-Mn-N5	101.745(143)
N2-Mn-O2	82.02(8)	N2-Mn-O2	83.45(10)	N2-Mn-N8	95.255(142)
N3-Mn-O3	82.98(8)	N3-Mn-O3	82.27(10)	N5-Mn-N8	102.503(142)

Table S2: Structural parameters for the Mn^{2+} local environment in the momometallated complex previously reported by Sunatsuki et al.,[2] the heterobimetallic complex **2** from this work, and the complex with the highest *D* value yet reported, a trigonal prismatic Mn^{2+} clatherochelate complex.[9] The high axial zero-field splitting was attributed to the local environment of the Mn^{2+} center in the clatherochelate complex. In complex **2** there is a similar geometry about the Mn^{2+} center, which should create a similar zero-field splitting to first-approximation. However, we observe a markedly higher zero-field splitting, which suggests that additional effects are contributing to *D*.

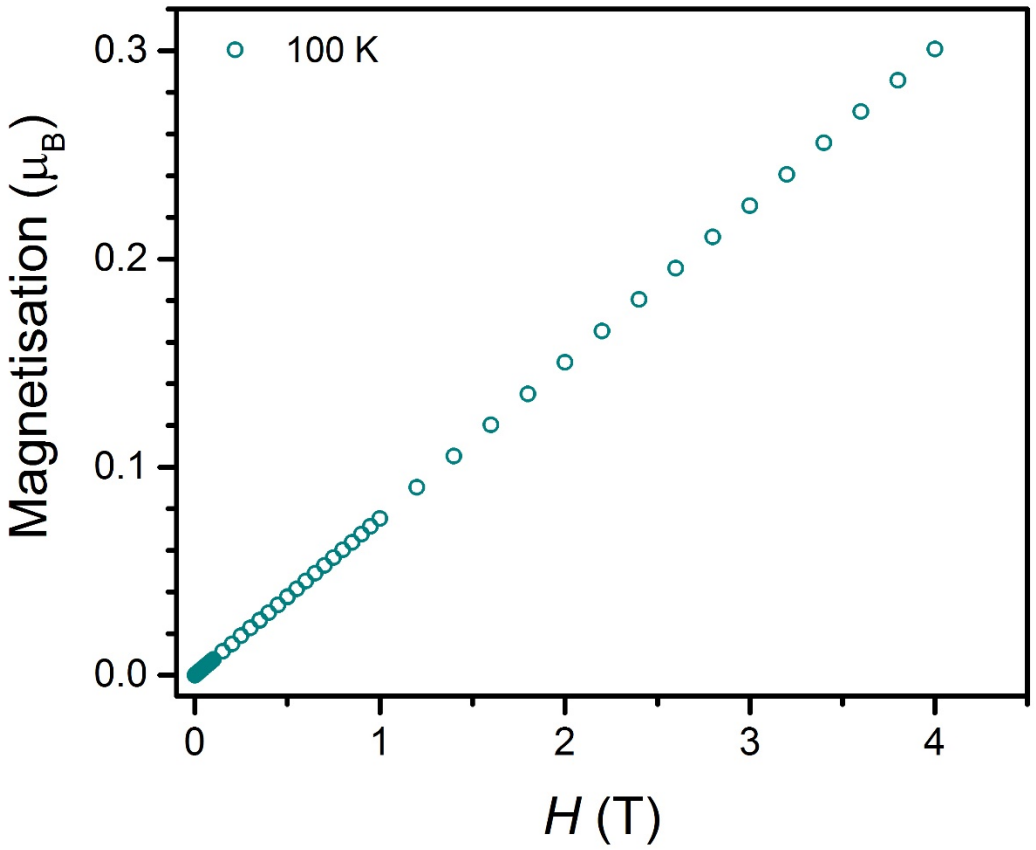

Figure S1: Variable field magnetization plot collected at 100 K. The linear behavior over all fields indicates the absence of ferromagnetic impurities in the sample.

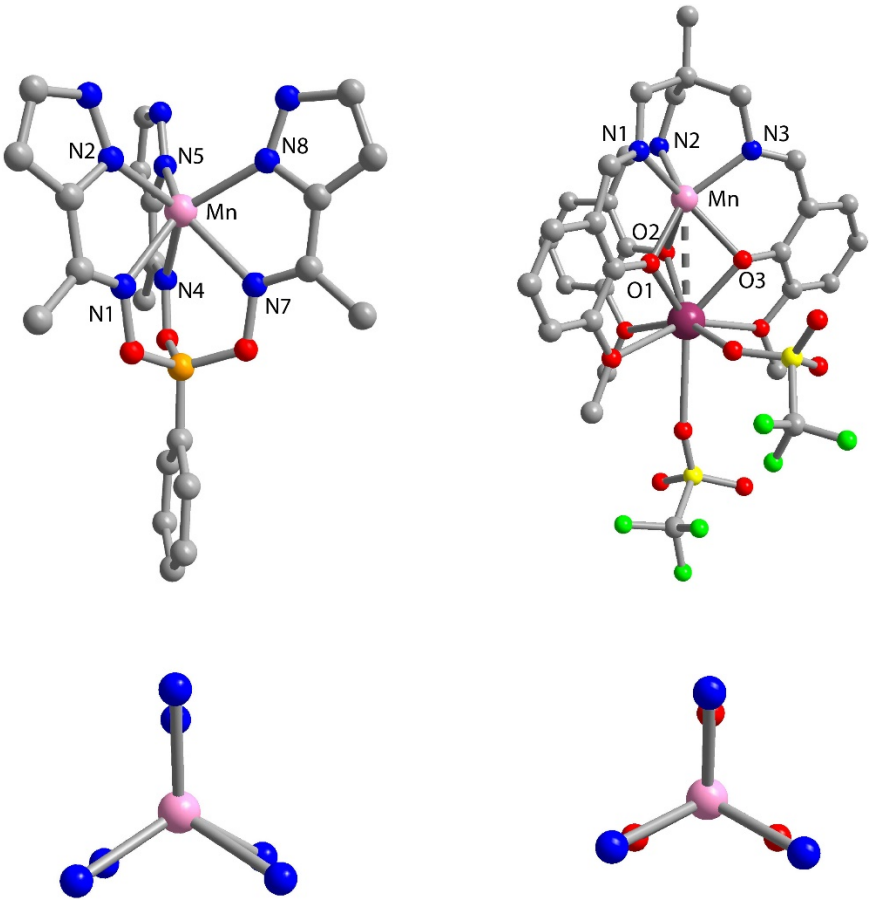

Figure S2: Left, a Mn^{2+} clatherochelate, which exhibits a *D* value of -0.32 cm^{-1}.[9] The metrics of the Mn^{2+} environment are tabulated in Table **S2**. The two structures both feature nearly idealized trigonal prismatic geometries, which should result in similar values for *D* if only ligand field effects are considered. The significant deviation in *D* values between the two structures indicates that additional spin-orbit effects play into the observed anisotropy in complex **2**.

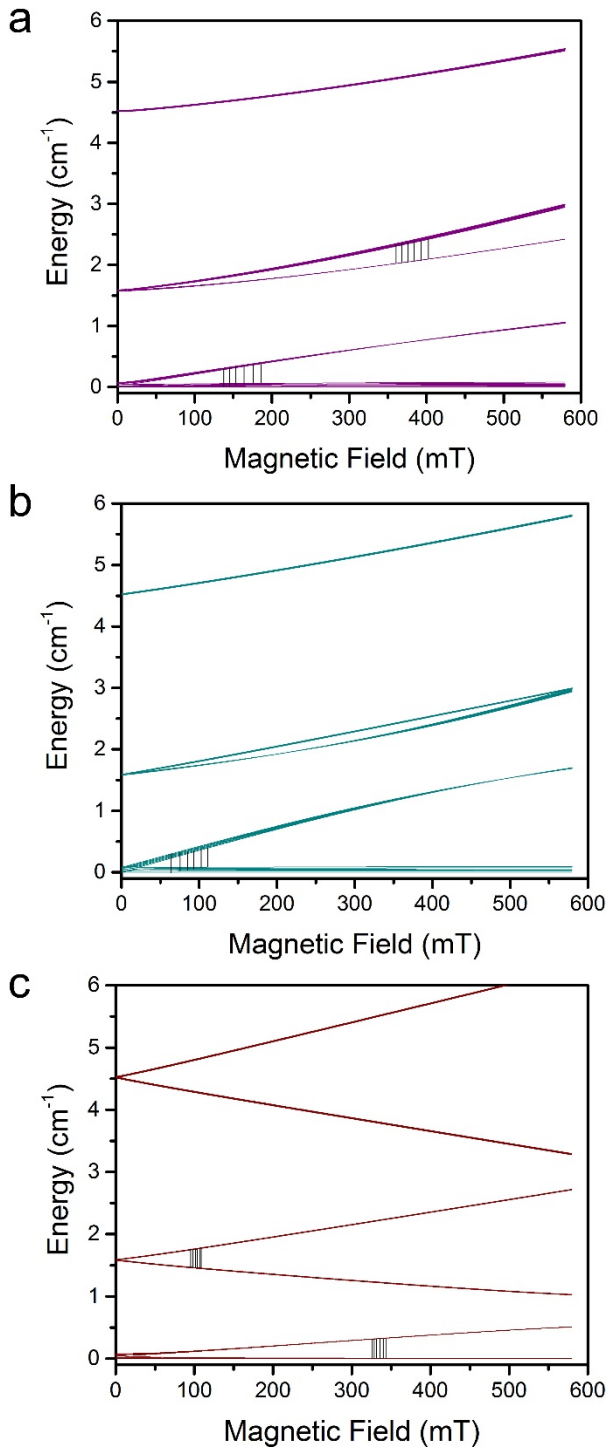

Figure S3: Zeeman plots for complex **2** along the (a) *x*, (b) *y*, and (c) *z* axes as calculated based on the parameters found by simulating the cw-EPR spectrum. The plots are normalized to the ground state. The observed transitions are shown as black lines. Hyperfine states are included in each plot and every hyperfine transition is shown separately. The hyperfine transitions are extremely close together in the *z*-direction but are distinct. These plots were calculated by EasySpin using the parameters outlined in the main text.[4]

References

1 Qin, C.; James, L.; Chartres, J. D.; Alcock, L. J.; Davis, K. J.; Willis, A. C.; Sargeson, A. M.; Bernhardt, P. V.; Ralph, S. F. *Inorg. Chem.* **2011**, 50, 9131–9140.

2 Sunatsuki, Y.; Kishima, Y.; Kobayashi, T.; Yamaguchi, T.; Suzuki, T.; Kojima, M.; Krzystek, J.; Sundberg, M. R. *Chem. Commun.* **2011**, 47, 9149-9151.

3 DAVE: A comprehensive software suite for the reduction, visualization, and analysis of low energy neutron spectroscopic data, R. T. Azuah, L. R. Kneller, Y. Qiu, P. L. W. TregennaPiggot, C. M. Brown, J. R. D. Copley, and R. M. Dimeo, *J. Res. Natl. Inst. Stan. Technol.* **2009**, 114, 341-358.

4 EasySpin, a comprehensive software package for spectral simulation and analysis in EPR *J. Magn. Reson.* 178(1), 42-55 (2006).

5 APEX2, v. 2014 ; Bruker Analytical X-Ray Systems, Inc: Madison, WI, 2014.

6 Sheldrick, G. M. SADABS, Version 2.03; Bruker Analytical X-Ray Systems, Inc.: Madison, WI, 2000.

7 Sheldrick, G. M. SHELXTL, Version 6.12; Bruker Analytical X-ray Systems, Inc.: Madison, WI, 2000.

8 Dolomanov, O. V.; Bourhis, L. J.; Gildea, R. J.; Howard, J. A. K.; Puschmann, H. J. Appl. Cryst. 2009, 42, 339–341.

9 Azarkh, M.; Penkova, L. V.; Kats, S. V.; Varzatskii, O. A.; Voloshin, Y. Z.; Groenen, E. J. J. J. Phys. Chem. Lett., 2014, 5, 886–889.